Applied Catalysis B: Environmental 234 (2018) 329–336

Contents lists available at ScienceDirect

Applied Catalysis B: Environmental

journal homepage: www.elsevier.com/locate/apcatb

Pt-modified TaC as an efficient electrocatalyst for ethanol oxidation in acid and alkaline electrolytes

Zhao Jiang[a,b,1], Qian Zhang[b,1], Zhixiu Liang[c], Jingguang G. Chen[b,c,*]

[a] Department of Chemical Engineering, Xi'an Jiaotong University, Xi'an, 710049, China
[b] Department of Chemical Engineering, Columbia University, New York, NY 10027, USA
[c] Chemistry Department, Brookhaven National Laboratory, Upton, NY, 11973, USA

ARTICLE INFO

Keywords:
Ethanol oxidation reaction (EOR)
Platinum-modified tantalum carbide (TaC)
In-situ infrared reflection absorption spectroscopy (IRRAS)
Density functional theory (DFT)

ABSTRACT

Ethanol is an ideal fuel in low-temperature fuel cells. The ethanol oxidation reaction (EOR) on platinum-modified tantalum carbide (TaC) has been investigated using both model thin films and powder catalysts. The results demonstrate that the 1.5 wt% Pt-modified TaC catalyst shows enhanced EOR activity compared to Pt. *In-situ* infrared reflection absorption spectroscopy (IRRAS) study reveals that the Pt surface is less poisoned by EOR intermediates and a higher CO_2 selectivity (7 ~ 9%) is achieved on the 1.5 wt% Pt/TaC catalyst, compared to the 40 wt% Pt/C. Density functional theory (DFT) calculations reveal that the binding energies of EOR intermediates on the Pt/TaC(111) surface are weaker than on Pt(111), suggesting an enhanced poison-tolerance from the adsorption of these intermediates. The combined experimental and theoretical investigations indicate that Pt/TaC is a promising electrocatalyst for EOR.

1. Introduction

Increasing energy demand and environmental concerns of continuous fossil fuel consumption have stimulated alternative energy research [1–3]. Low-temperature fuel cells have attracted extensive attention due to their high efficiency and broad applications in the transportation sector [4]. Although hydrogen fuel cells have been studied extensively [5], the utilization of hydrogen faces challenges in storage and transportation [6]. Oxygenates, such as methanol and ethanol, can generate energy in direct alcohol fuel cells (DAFCs). They are more commercially favored over hydrogen due to the compatibility with the existing storage and transportation infrastructure [7]. Ethanol has several advantages over methanol, including higher specific energy density and non-toxicity. Ethanol also has competitive market prices due to mass production from a variety of feedstocks [8–10].

The most promising and active catalysts for the ethanol oxidation reaction (EOR) in DAFCs are Pt and Pt-based alloys (e.g. Pt-Ru) [3]. However, the carbonyl-containing and/or carbon monoxide (CO) intermediates bind strongly to Pt surfaces and poison the catalysts at low potentials (*e.g.*, below 0.6 V vs. RHE) [11,12]. Higher operating potentials can avoid poisoning but decrease the cell efficiency. Additionally, the scarcity of Pt-group metals potentially prevents Pt-group catalysts from being commercialized on a large scale [13]. Supporting Pt on transition metal carbides (TMC) has shown promise in alleviating these problems. For example, monolayer (ML) Pt supported on tungsten carbide (WC) has shown an enhanced CO tolerance by reducing the CO binding energy on Pt/WC [14–17], which would potentially enhance the EOR activity. ML Pt/TMCs can also significantly reduce the Pt loading in electrocatalysts [18,19].

Although ML Pt/WC has shown good EOR performance in acid [17], WC would be oxidized at higher voltages in alkaline electrolyte [20], making it unsuitable for alkaline EOR. Given the fact that EOR activities on Pt are reported to be several orders of magnitude higher in alkaline than in acid [21,22], it is important to explore stable Pt-modified TMC catalysts for alkaline EOR. Tantalum carbide (TaC) is a qualified candidate due to its higher stability than WC in alkaline [20]. It is possible that TaC increases the hydroxyl adsorption capacity and thus facilitates the oxidation of CO with adsorbed OH. It has been reported in literature that the formation of adsorbed hydroxyl over TMC is thermodynamically favored in both experiments and DFT calculations [23–25]. In this work, EOR activity of ML Pt/TaC thin films and 1.5 wt % Pt/TaC powder catalysts were measured by electrochemical methods. The stability was examined by X-ray photoelectron spectroscopy (XPS) measurements for pre- and post- testing thin film samples. The EOR mechanism on Pt/TaC was further investigated by *in-situ* infrared reflection absorption spectroscopy (IRRAS) and density

* Corresponding author at: Chemistry Department, Brookhaven National Laboratory, Upton, NY, 11973, USA.
E-mail address: jgchen@columbia.edu (J.G. Chen).
[1] These authors contributed equally to this work and should be regarded as co-first authors.

https://doi.org/10.1016/j.apcatb.2018.04.052
Received 15 February 2018; Received in revised form 20 April 2018; Accepted 22 April 2018
Available online 23 April 2018
0926-3373/

functional theory (DFT) calculations.

2. Experimental and theoretical methods

2.1. Synthesis and characterization of ML Pt/TaC thin films

Ta foils (Alfa Aesar, 0.25 mm thick annealed 99.95%) were rinsed in acetone and deionized (DI) water followed by being soaked in 0.3 M NaOH for 15 min to remove impurities. They were inserted into a quartz tube furnace in a gas flowing environment of 100 mL min^{-1} H_2 and 20 mL min^{-1} CH_4. The Ta foils were slowly heated to 1273 K and kept at the temperature for one hour to carburize the foils, using a temperature ramping procedure described in literature [20]. After the carburization, the temperature was held at 1123 K for 30 min with a flow of 100 mL min^{-1} H_2 to remove excess surface carbon [26]. The furnace was gradually cooled down for eight hours in a reduced flow of 70 mL min^{-1} H_2 followed by the passivation in a flow of 30 mL min^{-1} 1% O_2/99% N_2 for one hour at room temperature. Pt physical vapor deposition (PVD) on TaC thin films was performed in an ultra-high vacuum (5×10^{-9} Torr) system equipped with XPS. The Pt PVD process and XPS fitting procedures for peak integrations were described in previous work [19].

Scanning electron microscope (SEM) images were taken using a SEISS SEM for examining surface morphology with an accelerating voltage of 6 kV. The thin film characterization results including XPS spectra for pre- and post-carburization are shown in Fig. S1.

2.2. Synthesis and characterization of 1.5 wt% Pt/TaC catalyst

The wet impregnation method was used to synthesize 1.5 wt percent (wt%) Pt on commercial TaC (Sigma-Aldrich) catalyst. A target amount of $Pt(NH_3)_4(NO_3)_2$ (Tetra-ammine-platinum(II)nitrate from Sigma-Aldrich) as the Pt precursor was dissolved in 10 ml of DI water. The solution was then agitated at room temperature (RT) for five hours with a magnetic stirrer. Then 200 mg commercial TaC powder were added slowly while the solution continued stirring. After twelve hours, the solution was dried on the stirrer at 383 K in air for five hours followed by calcination in a 40 mL min^{-1} H_2 flow environment. The temperature was raised to 673 K with a ramping rate of 2 K min^{-1} and held for one hour. The sample was cooled to RT under the same gas environment and then passivated in 1% O_2/99% N_2 for half an hour.

The characterization procedures and results for X-ray diffraction (XRD), transmission electron microscope (TEM) and copper underpotential deposition (UPD) stripping for calculating electrochemical surface area (ECSA) are described in the SI.

2.3. Electrochemical measurements and stability tests

Regarding working electrode preparation for thin films, 1 cm^2 geometric surface area was defined with electroplating tape with the backsides completely covered. To make catalysts ink, 1.5% Pt/TaC catalyst and commercial benchmarking 40 wt% Pt/Vulcan carbon were dissolved in calculated amount of water, isopropanol and Nafion 117 solution. Appropriate amount of ink was dropped on glassy carbon electrodes.

Electrochemical testing for ethanol oxidation were carried out at RT in acid (0.05 M H_2SO_4) and alkaline (0.1MKOH) electrolytes. Princeton Applied Research Versa STAT 4 was used as a potentiostat to conduct cyclic voltammetry (CV) and chronoamperometry (CA) testing. Electrochemical measurements were carried out with, and without 1 M ethanol (CH_3CH_2OH) in a three-electrode, single-cell set-up with graphite (Sigma-Aldrich, 99.995% purity) as a counter electrode and a reversible hydrogen electrode (RHE, Hydroflex) as a reference electrode. The working electrode was first cycled in Ar-purged pure acid or base without the presence of ethanol in a cyclic voltammetry (CV) between 0.1 and 1 V vs. RHE using a scan rate of 50 mV s^{-1}. The purpose of the CV scans in pure high (pH = 13) or low (pH = 1) pH electrolyte was to clean the electrode surface. Then EOR CV testing was conducted in the presence of ethanol at a scan rate of 50 mV s^{-1} for 20 scans in the range of 0.1 to 1 V vs. RHE. The 20th scan was used in this manuscript. After the CV testing, chronoamperometry (CA) testing was applied at a potential of 0.6 V vs. RHE for one hour. The cell resistance was measured at the beginning of the CV scan by using electrochemical impedance spectroscopy (EIS). All reported potentials were corrected by the cell resistance accordingly. After the thin film surfaces were tested, the sample was taken out from the solution and cleaned with DI water. After being dried, the post-testing samples were put into the UHV system for XPS measurements.

The electrochemical linear scanning voltammetry (LSV) for working electrodes made from powder samples was conducted in acid and alkaline ethanol electrolyte at the scan rate of 50 mV s^{-1}. CA testing followed the same procedure as described above for model thin films. The rotation rate of 1000 rotations per mins (rpm) was used for on glassy carbon electrode with deposited powder ink. The current densities for the powder catalysts were corrected by the cell resistance and normalized by their respective ECSA based on copper UPD.

2.4. In-situ infrared reflection absorption spectroscopy (IRRAS)-LSV

In-situ IRRAS-LSV measurements were carried out with a Nicolet iS50 FT-IR spectrometer equipped with an A-type MCT detector cooled with liquid nitrogen. The working electrode were made from depositing the appropriate amount of 1.5 wt% Pt/TaC catalyst ink or commercial 40 wt% Pt/C ink on glassy plates. Pt loadings were kept the same on the glassy plates for fair comparisons. Electrolytes contained either 0.05 M H_2SO_4/1 M ethanol or 0.1 M KOH/1 M ethanol. In both acid and alkaline electrolytes, sample spectra were collected from 0.05 V to 1 V vs. RHE at a scan rate of 1 mV s^{-1}. The details regarding the apparatus parameter setting and operating procedures are described in the SI.

2.5. DFT calculations

DFT calculations were carried out using the Vienna *Ab-Initio* Simulation Package (VASP) code [27]. The electronic ion interaction was modeled by the projector augmented wave (PAW) method [28]. The Perdew-Wang-91 (PW91) functional [29] with the generalized gradient approximation was employed to deal with the electronic exchange and correlation. The kinetic wave cutoff energy was set at 400 eV to describe the electronic wave functions. The Brillouin-zone integration was sampled using a $3 \times 3 \times 1$ Monkhorst-Pack k-points grid with a Gaussian smearing of 0.1 eV. The Pt(111) and Pt/TaC(111) surfaces were modeled by a four-layer 3×3 super-cell with the coverage of selected adsorbates of 1/9 monolayer. For the Pt/TaC(111) surface, a Pt monolayer was deposited on the TaC(111) surface. The bottom two layers were fixed, and the top layers were allowed to relax. A vacuum layer of 15 Å was added perpendicular to the slab to avoid artificial interactions between the slab and its periodic images.

The binding energies (BE) for all intermediates on the surfaces are defined as follows:

$$BE = E_{adsorbate/surface} - E_{adsorbate} - E_{surface} \quad (1)$$

where $E_{adsorbate/surface}$ is the total energy of the adsorbate together with the surface, $E_{adsorbate}$ is the total energy of the free adsorbate in the gaseous phase, and $E_{surface}$ is the total energy of the surface.

3. Results and discussion

3.1. Electrochemical studies of Pt/TaC thin films

The Pt-modified TaC thin films were prepared as model surfaces for electrochemical and stability testing. The CV results for 1 ML Pt-modified TaC surfaces in 0.05 M H_2SO_4 and 0.1 M KOH are shown in Fig. 1A

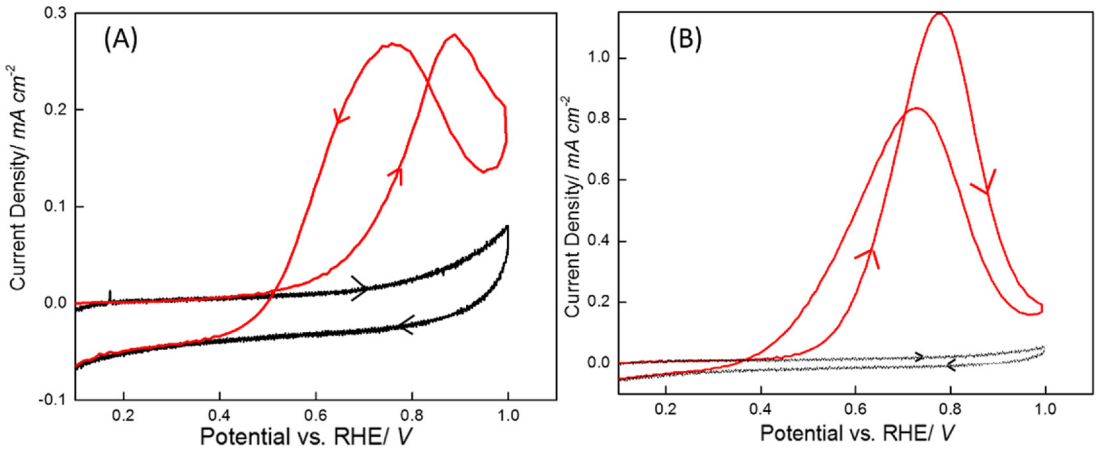

Fig. 1. CV scans for 1 MLs Pt/TaC at a scan rate of 50 mV S^{-1}, shown in red collected in 0.05 M H_2SO_4/1 M ethanol while the CV scan shown in black collected in only 0.05 M H_2SO_4 (A); shown in red collected in 0.1 M KOH/1 M ethanol while the CV scan shown in black collected in only 0.1 M KOH (B); The arrow indicating the corresponding part of each plot to forward scan and backward scan, respectively (For interpretation of the references to colour in this figure legend, the reader is referred to the web version of this article).

and B, respectively. The CV results in acid and alkaline solutions without ethanol showed no oxidation peaks, indicating that 1 ML Pt/TaC was stable at least up to 1 V *vs.* RHE. In the presence of 1 M ethanol in acid or alkaline electrolyte, two distinctive peaks were observed in the forward (anodic) and reverse (cathodic) scans for the Pt/TaC surfaces, characteristic of ethanol oxidation [12,21,30].

In order to compare the activity of Pt-modified TaC with different Pt coverage, EOR CA results for 0.5 ML, 1.0 ML, 2.0 ML Pt-modified TaC and Pt polycrystalline surfaces in acid and alkaline are compared in Fig. 2. The acid EOR steady-state current density obtained at the potential of 0.6 V vs. RHE for one hour (Fig. 2A) indicated that the activity increased along with an increase in the number of Pt overlayers. Among all tested samples, the highest activity was obtained by 2 ML Pt/TaC in acid. The 1 ML Pt/TaC film exhibited equivalent EOR activity as the Pt film. The current density in Fig. 2 was normalized by geometric surface area of the low surface area thin films rather than their ECSAs, because it was difficult to use traditional ECSAs measurement methods (e.g. Copper stripping or H- UPD) to obtain statistically meaningful results for the low surface area Pt/TaC thin films. The ECSA-normalized EOR activity comparison for Pt-modified TaC and Pt bulk is later discussed in high surface area powder catalysts.

In alkaline (Fig. 2B) the activity for 1 and 2 ML Pt/TaC showed similar steady-state activity as the polycrystalline Pt film, while an unmodified TaC surface resulted in no EOR. The comparison of steady-state EOR current density in acid (Fig. 2A) and alkaline (Fig. 2B) indicated that the high pH environment resulted in an enhanced EOR activity. At 0.6 V vs. RHE, the EOR activity for the 2 ML Pt/TaC surface was 110 μA cm^{-2} in alkaline while it was only 35 μA cm^{-2} in acid. The enhanced EOR activity in alkaline was also reported on the Pt surface. The enhanced EOR activity for the MLs Pt/TaC surfaces in high pH may be attributed to the ease of ethoxy formation and the high hydroxide (OH^-) concentration as oxygen-donating species [12,21,22,31]. The absence of bisulfate poisoning in alkaline electrolyte should also result in enhanced EOR activity [32,33].

The XPS results for the model surfaces pre- and post- electrochemical testing in both acid and alkaline environments were compared to evaluate the electrochemical stability, shown in Fig. 3. Comparisons of the ratios of Pt4f to Ta4f integrated areas for pre- and post- electrochemical testing resulted in a decrease by approximately10% after the testing. Such a small decrease in the Pt/Ta ratios could likely be attributed to screening by the adsorption of electrolytes on the surface [34]. The relatively small changes in the Pt/Ta ratios suggested that the Pt overlayers were stable for EOR in both acid and alkaline electrolytes.

The Ta4f XPS spectra for 0.5 ML Pt/TaC and 1 ML Pt/TaC pre- and post- EOR testing are compared in Fig. 3C and D. The peaks at 22.62 eV and 24.53 eV corresponded to TaC, while the peaks at 25.21 eV and

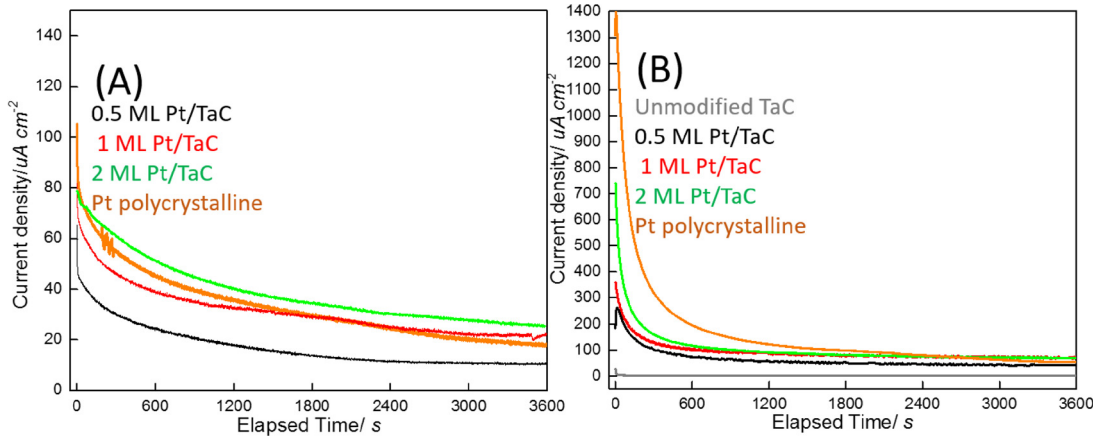

Fig. 2. CA scans (A) in 0.05 M H_2SO_4/1 M ethanol and CA scans (B) in 0.1 M KOH/1 M ethanol of 0.5 ML Pt/TaC at 0.6 V v.s RHE for one hour; The catalyst of unmodified TaC shown in grey color, 0.5 ML Pt/TaC in black, 1 ML Pt/TaC in green, 2 ML Pt/TaC in red and Pt bulk in orange; The current densities were normalized by the geometric surface area of the TaC thin films (For interpretation of the references to colour in this figure legend, the reader is referred to the web version of this article).

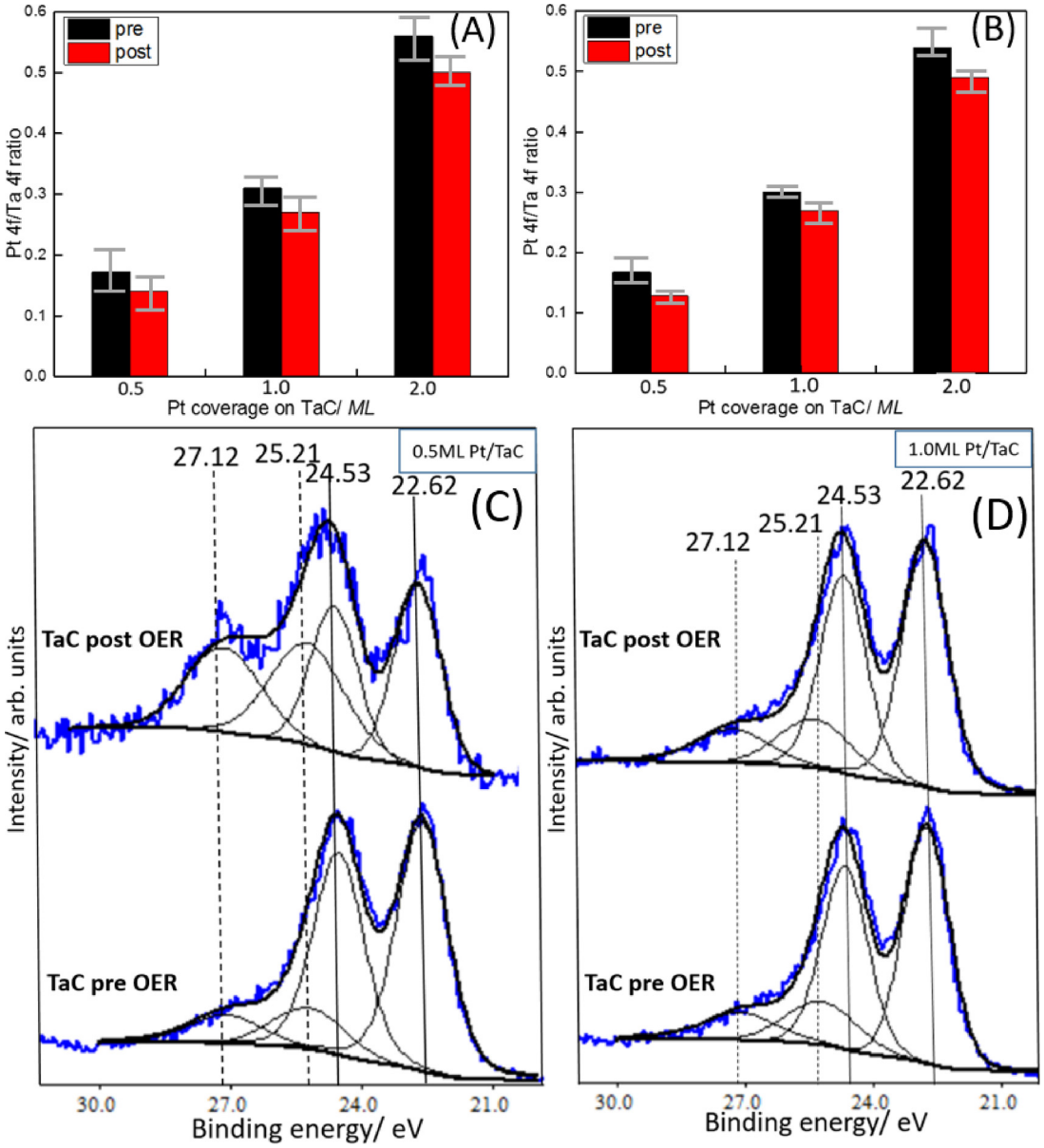

Fig. 3. The ratio of Pt4f to Ta4f integrated areas from XPS measurements for pre- and post- EOR electrochemical testing for different ML Pt/TaC in acid (A) and base (B). XPS Ta4f spectra for pre- and post- EOR stability testing in base for 0.5 ML Pt/TaC (C) and 1 ML Pt/TaC (D). Electrochemical testing including 20 times CV scans followed by one-hour CA testing at 0.6 V vs. RHE CV measurements.

27.12 eV correlated to oxidized Tas. The observation of surface oxide peaks in the fresh samples was expected due to the passivation process after TaC synthesis. Further oxidization occurred during the electrochemical testing in 0.5 ML Pt/TaC, likely due to the oxidation of uncovered TaC during EOR testing. In contrast, XPS results of the post-testing 1 ML Pt/TaC (Fig. 3D) showed that TaC was not further oxidized, indicating that deposited ML Pt prevented the TaC substrate from being oxidized. Overall, the results in Fig. 3 indicated that the ML Pt/TaC film was electrochemically stable for EOR under acid and alkaline conditions.

3.2. Electrochemicalstudies of 1.5 wt% Pt/TaC powder catalysts

Because high surface area powder catalysts are more industrially relevant, 1.5 wt% Pt/TaC and the benchmark commercial 40 wt% Pt/C catalysts were studied by electrochemical LSV and CA testing in both acid and alkaline, shown in Fig. 4. In order to account for the Pt dispersion effect on the EOR activity, the current density was normalized by the electrochemical surface areas (ECSAs) of both catalysts. The copper UPD stripping results for determining the ECSAs of the two samples are described in Fig. S2.

As shown in Fig. 4A, enhanced LSV current density was achieved in 1.5 wt% Pt/TaC compared to that of 40 wt% Pt/C. Although the onset potential was similar for the two catalysts in acid, the LSV current density of 1.5 wt% Pt/TaC was significantly higher at 0.6 V. The enhanced acid EOR activity for 1.5 wt% Pt/TaC was further illustrated in the CA results (Fig. 4B). 1.5 wt% Pt/TaC achieved 0.7 mA cm^{-2} compared to 0.028 mA cm^{-2} for 40 wt% Pt/C at 0.6 V vs. RHE. The same trends were observed in alkaline as in acid. The 1.5 wt% Pt/TaC catalyst increased current density more rapidly than 40 wt% Pt/C in the LSV (Fig. 4C) and had higher current density at 0.6 V vs. RHE (Fig. 4D).

In order to uncover underlying reasons for the enhanced activity obtained by 1.5 wt% Pt/TaC compared to 40 wt% Pt/C, *in-situ* IRRAS-LSV experiments under the acid and alkaline EOR conditions were performed to identify the EOR intermediates and final products at different potentials. The difference in onset potentials from

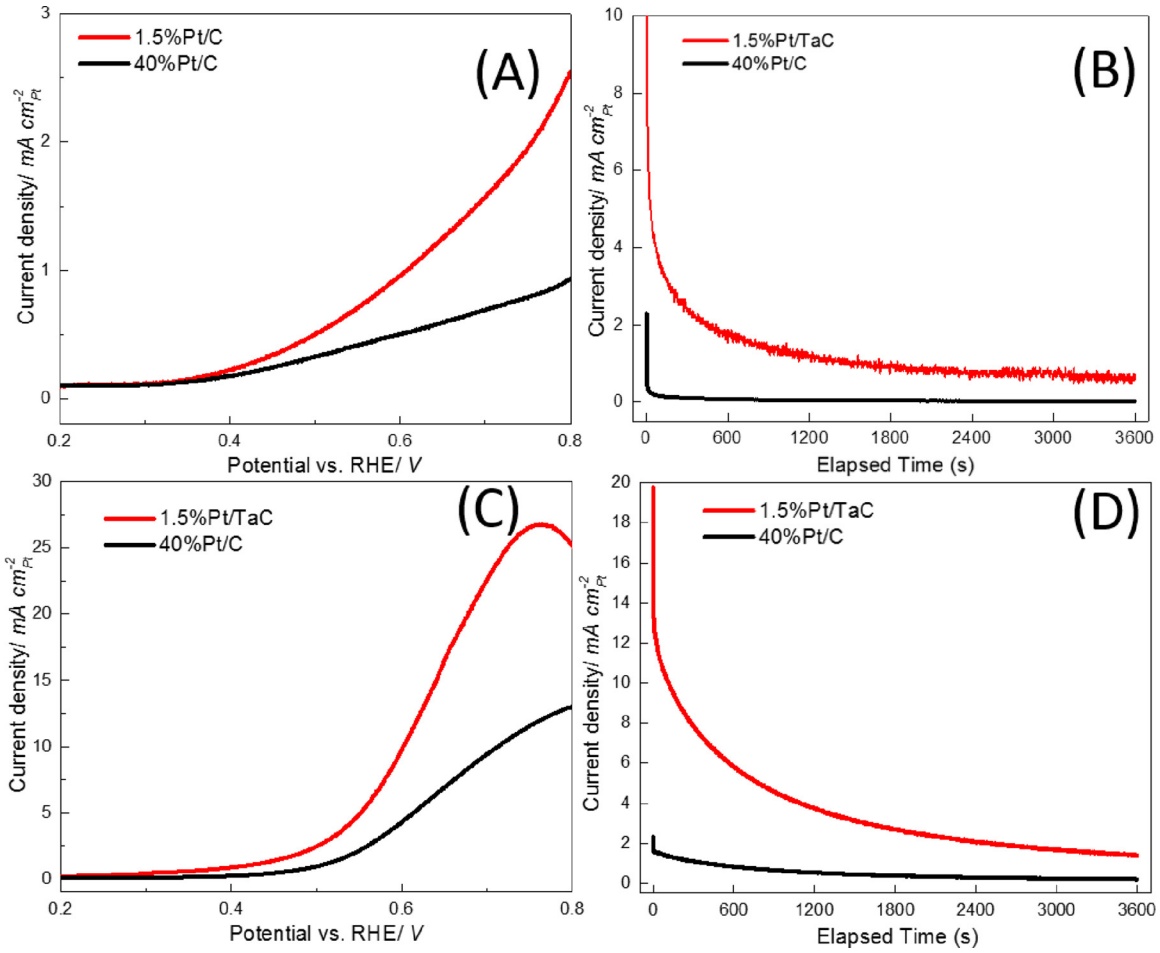

Fig. 4. LSV scans (A) and one-hour CA testing at 0.6 V vs. RHE (B) for 1.5 wt% Pt/TaC shown in red color and commercial 40 wt% Pt/C shown in black colour in 0.5 M H_2SO_4/1 M EtOH; LSV scans (C) and one-hour CA testing at 0.6 V vs. RHE (D) in 0.1 M KOH/1 M EtOH. The current density was normalized by their respective Pt ECSA of 1.5 wt% Pt/TaC and commercial 40 wt% Pt/C (For interpretation of the references to colour in this figure legend, the reader is referred to the web version of this article).

electrochemical LSV testing (Fig. 4A and C) and *in-situ* IRRAS-LSV testing (Figs. 5A, B and 6) can be explained by the differences in transport conditions and difference scan rates. Although it is not suitable to directly compare the quantitative results obtained from the electrochemical LSV testing and the *in-situ* IRRAS-LSV experiment, the qualitative trend should remain valid.

For 40 wt% Pt/C in acid (Fig. 5A), vibrational modes associated with acetic acid (CH_3COOH) (νs(C—O) at 1280 cm^{-1} and ν(C═O) at 1715 cm^{-1}) and acetaldehyde (CH_3CHO), (νasC-C-O) at 933 cm^{-1} and ω(C–H) at1108 cm^{-1}) [36,37] were detected. At the same time, downward features, ν(C–O) at 1044 cm^{-1} [38] for ethanol and δ((H—O—H) at 1635 cm^{-1} [38] for water, indicated that these two molecules were consumed. The C_1 product, carbon dioxide (CO_2), νas (C—O—O) mode at 2341 cm^{-1} [12,39,40], was produced at 0.65 V *vs.* RHE. The peak assignments for 40 wt% Pt/C matched well with previous reports [41]. All peaks assignments can be found in SI. The C_1 and C_2 peaks both started at the potential of 0.65 V, indicating a parallel reaction pathway for C_1 and C_2. Regarding the C_1 reaction pathway, adsorbed carbon monoxide, ν(CO) at 2041 cm^{-1}, from the C—C bond scission was observed starting at 0.38 V vs. RHE and the peak area continued to increase along with an increase in applied potential until 0.65 V. This indicated that adsorbed CO remained on the Pt surface until a potential of 0.65 V was reached. Starting from 0.65 V, the CO_2 feature at 2341 cm^{-1}, the C_1 reaction pathway final product, was observed. The peak area of the 2341 cm^{-1} mode then grew with increasing potentials while the peak area of the CO feature at 2041 cm^{-1} started decreasing. Regarding the C_2 reaction pathway, the C_2 oxidation products (CH_3CHO and CH_3COOH) were detected at a potential of 0.65 V.

On 1.5 wt% Pt/TaC, the IR peaks for acetaldehyde, acetic acid, and carbon dioxide were also observed. Other peaks associated with C_1 and C_2 species are listed in the Table S1 of the SI. The EOR reaction pathways started at 0.47 V on 1.5 wt% Pt/TaC, which was approximately 0.2 V lower compared to that of 40 wt% Pt/C (Fig. 5 A). The adsorbed CO peak at 2041 cm^{-1} was not detected throughout the entire potential range on 1.5 wt% Pt/TaC, indicating that the adsorbed CO can be easily oxidized on the 1.5 wt% Pt/TaC surface, unlike that on 40 wt% Pt/C [42,43]. This suggested that the kinetics for the C_1 reaction pathway on 1.5 wt% Pt/C should not be limited by adsorbed CO intermediates. Therefore, enhanced current density on the 1.5 wt% Pt/TaC (Fig. 4C) was ascribed to faster kinetics due to higher tolerance to strongly adsorbed surface intermediates that poisoned the surface sites, as in the case of 40 wt% Pt/C.

The CO_2 (C_1) selectivity is defined as the ratio of distributed charge associated with CO_2 production to the total charge associated with the products from both C_1 and C_2 pathways. The C_1 selectivity for 1.5 wt% Pt/TaC and 40 wt% Pt/C were further quantified because the C_1 selectivity could be used to evaluate the catalytic efficiency for EOR. A higher C_1 selectivity represents a more efficient EOR catalyst. Among all products, the C_1 product (CO_2) is produced from the total ethanol oxidation as the most efficient reaction pathway and 12 mol electrons (highest faraday efficiency) are produced. In comparison, C_2 products

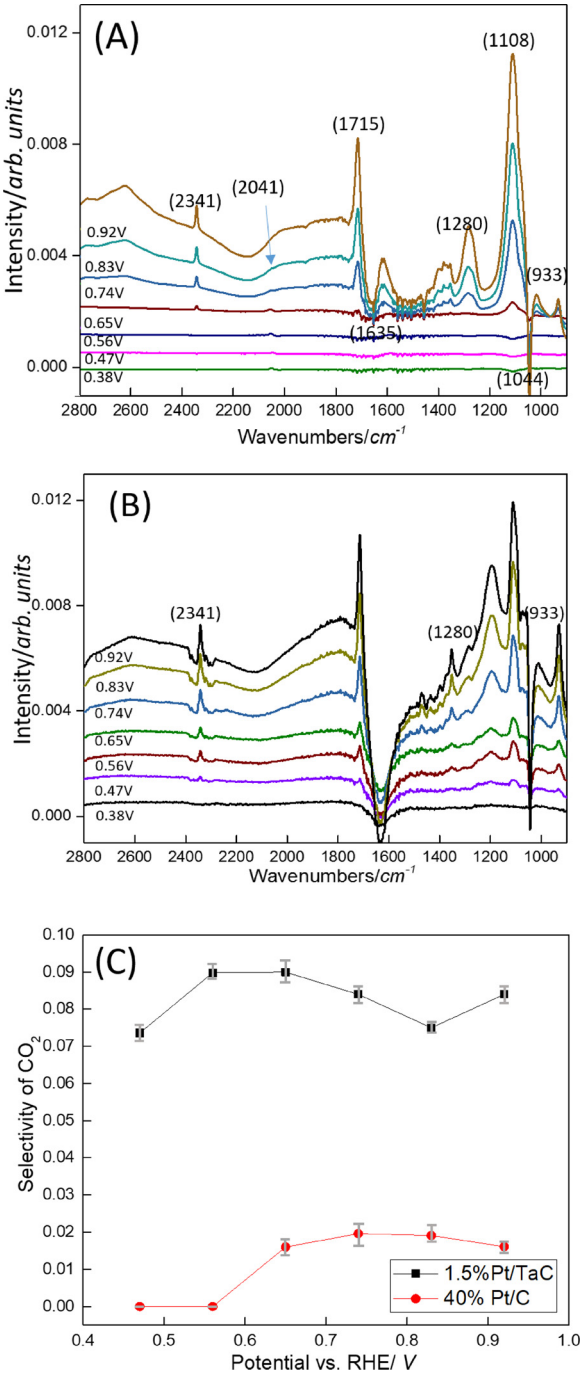

Fig. 5. In-situ IRRAS spectra of 40 wt% Pt/C (A) and of 1.5 wt% Pt/TaC (B) in acid EOR LSV testing; the selectivity of CO_2 along with applied potential (C) on 1.5 wt% Pt/TaC indicated in black squares and commercial 40 wt% Pt/C indicated in red circles. (For interpretation of the references to colour in this figure legend, the reader is referred to the web version of this article).

are from partial ethanol oxidation, with one mole ethanol oxidation only resulting in only 2 (CH_3CHO as the final product) or 4 (CH_3COOH as the final product) moles electrons. The integrated IR peak areas for acetaldehyde (933 cm^{-1}), acetic acid (1280 cm^{-1}), and CO_2 (2341 cm^{-1}) can be used to illustrate the qualitative trend for the C_1 species selectivity, as described in literature [44,45]. Based on the CO_2 selectivity for EOR on 40% Pt/C and 1.5% Pt/TaC in acid, shown in Fig. 5C, CO_2 was not produced on 40% Pt/C below 0.6 V and the peak area ratio was only 2% above 0.6 V. In comparison, the CO_2 peak area ratio on 1.5% Pt/TaC was 7–9% at potentials starting at 0.47 V,

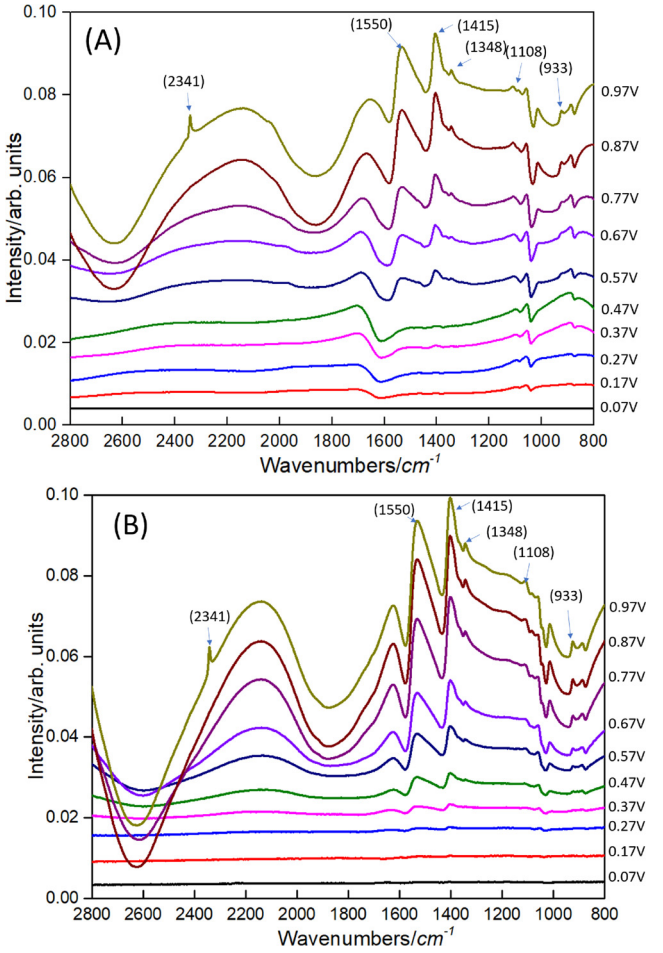

Fig. 6. In-situ IRRAS spectra of 40 wt% Pt/C(A) and of 1.5 wt% Pt/TaC (B) in alkaline EOR LSV testing.

indicating that this catalyst underwent a more efficient reaction pathway through the C—C bond breakage.

In-situ IRRAS-LSV experiments were also performed on 40 wt% Pt/C (Fig. 6A) and 1.5 wt% Pt/TaC (Fig. 6B) in alkaline electrolyte. On the 40% Pt/C catalyst, acetate (CH_3COO^-) in alkaline, instead of acetic acid in acid, was identified as the main C_2 product, as indicated by peaks of νas(O—C—O) at 1550 cm^{-1} and νs(O—C—O) at 1415 cm^{-1} [36,46] The other C_2 vibrational peaks, νas(O—C—O) at 933 cm^{-1} and ω(C–H) at 1108 cm^{-1}, were attributed to CH_3CHO. C_2 product peaks at 1550 cm^{-1} and 933 cm^{-1}peaks on 40 wt% Pt/C were detected starting at the potential of 0.57 V while the onset potential was lower starting at 0.37 V for 1.5 wt% Pt/TaC. Peaks assignments could be found in SI.

Regarding the C_1 reaction pathway, unlike the case in acid electrolyte, the product selectivity could not be compared in alkaline electrolyte due to the overlapping IR peaks of C_1 and C_2 products. The carbonate anion signal at 1390 cm^{-1} [46] and the bicarbonate signal at 1360 cm^{-1} [47], resulting from C_1 species in alkaline, were convoluted with the acetate bands at 1415 cm^{-1} and 1348 cm^{-1} [35,46]. The 2341 cm^{-1} CO_2 feature was supposed to be the C_1 EOR product in acid environment, but the CO_2 feature was detected starting at the potential of 0.97 V *vs.* RHE in alkaline on both catalysts (Fig. 6). This might be attributed to the neutralization of the electrolyte thin layer between the IR window and the working electrode [35].

3.3. DFT calculations

In order to further understand the electrochemical and *in-situ* IRRAS results, DFT calculations were performed to compare the binding

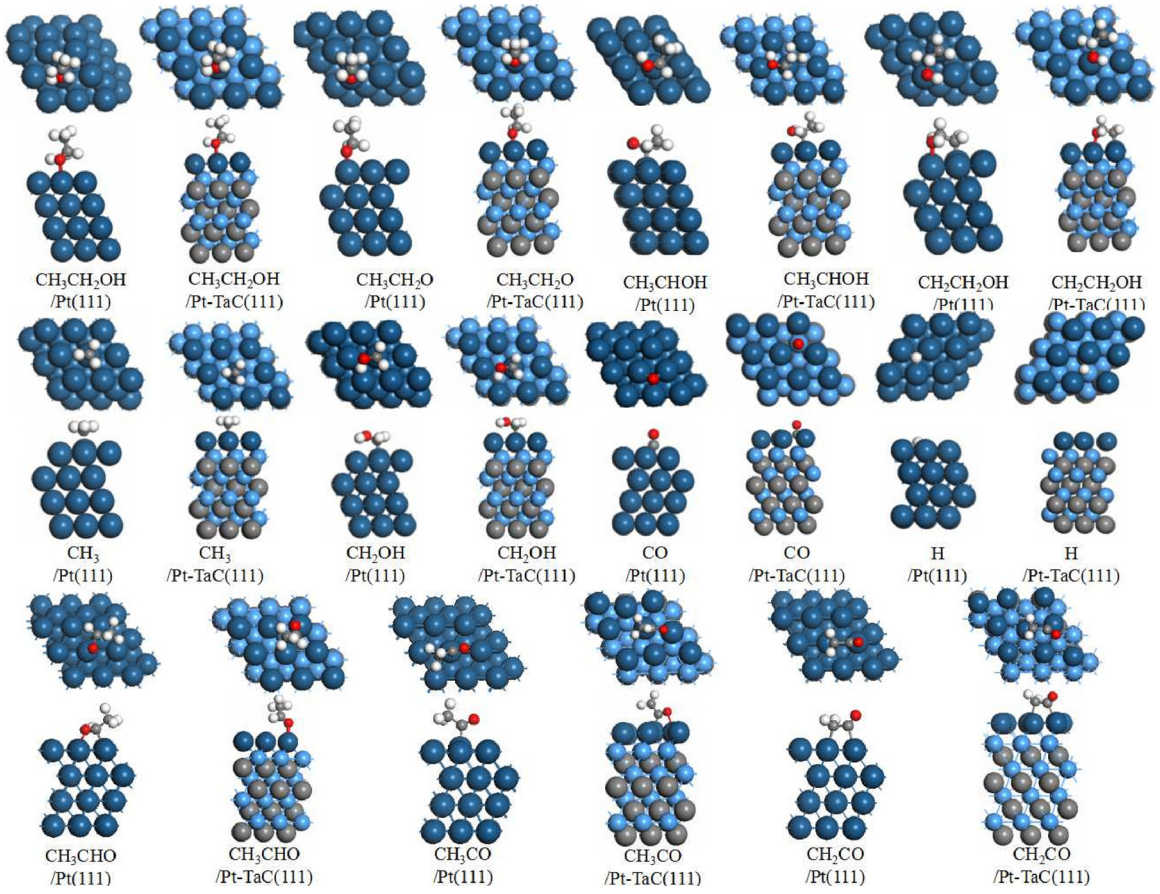

Fig. 7. Top and side views of the most stable configurations of the possible intermediates on Pt(111) and Pt/TaC(111) surfaces.

Table 1
DFT calculations of binding energies (eV) of potential EOR intermediates on Pt (111) and Pt/TaC(111) surfaces.

Surfaces	Species	Configurations	Binding energies/eV
Pt(111)	CH_3CH_2OH	atop, O-bound	−0.31
	CH_3CH_2O	atop, O-bound	−1.82
	CH_3CHOH	atop, C_α-bound	−2.28
	CH_2CH_2OH	atop, C_β –bound	−2.45
	CH_3	atop, C-bound	−2.38
	CH_2OH	atop, C-bound	−2.37
	CH_3CHO	bridge, C-bound and O-bound	−0.71
	CH_3CO	atop, C-bound	−2.37
	CH_2CO	bridge, C-bound	−1.48
	CO	fcc, C-bound	−2.02
	H	fcc, H-bound	−0.46
Pt/TaC(111)	CH_3CH_2OH	atop, O-bound	−0.42
	CH_3CH_2O	atop, O-bound	−1.92
	CH_3CHOH	atop, C_α-bound	−1.42
	CH_2CH_2OH	atop, C_β –bound	−1.92
	CH_3	atop, C-bound	−1.66
	CH_2OH	atop, C-bound	−1.50
	CH_3CHO	atop, O-bound	−0.48
	CH_3CO	atop, C-bound	−1.90
	CH_2CO	bridge, C-bound	−0.51
	CO	hcp, C-bound	−1.35
	H	bridge, H-bound	−0.28

energies of the intermediates from C—C and C—H bond scissions in ethanol on Pt(111) and Pt/TaC(111) surfaces. Based on the EOR mechanism proposed in the reports [48,49] the possible surface intermediates included CH_3CH_2OH, CH_3CH_2O (ethoxy), CH_3CHOH, CH_2CH_2OH, CH_3, CH_2OH, CH_3CHO, CH_3CO, CH_2CO and CO. The high symmetry adsorption sites of both surfaces were considered: atop, bridge, fcc, and hcp sites. The most stable adsorption configurations of these possible intermediates on Pt(111) and Pt/TaC(111) surfaces are shown in Fig. 7. The binding energies and key geometric parameters of all the species at the most stable positions are listed in Table 1. Furthermore, partial density of states (PDOS) of Pt d-states in Pt(111) and Pt/TaC(111) were calculated. It was found that the interaction between TaC and Pt modified the electronic structures of Pt (Fig. S6 in the Supporting Information), consistent with a previous previous study of Pt on tungsten carbide [50].

As shown in Fig. 7, ethanol preferred to bind at the atop site on both surfaces. The ethanol interaction with Pt/TaC(111) was slightly stronger than Pt(111) with the binding energy of −0.42 eV and −0.31 eV, respectively. The binding energy of ethoxy was also slightly higher on Pt/TaC (-1.92 eV) than that on Pt (−1.82 eV). Interestingly, for other intermediates (CH_3CHOH, CH_2CH_2OH, CH_3, CH_2OH, CH_3CHO, CH_3CO, CH_2CO and CO), the binding energies on the Pt/TaC(111) surface were smaller than those on the Pt(111) surface, suggesting that Pt/TaC(111) should have a higher tolerance to the site-blocking by EOR intermediates, agreeing well with the *in-situ* IRRAS-LSV results. For example, the CO binding energies were calculated to be -2.02 and -1.35 eV on the Pt(111) and Pt/TaC(111) surfaces, respectively. The higher CO binding energy on the Pt(111) surface by 0.67 eV indicated that Pt sites are more likely to be blocked by CO on the Pt (111) surface [42,43], which required higher potential to oxidize the adsorbed CO. On the other hand, the lower CO binding energy on Pt/TaC suggested that the CO poisoning effect was alleviated on the Pt/TaC surface, resulting in more facile CO oxidation on Pt/TaC, in agreement with the observation in *in-situ* IRRAS-LSV (Fig. 5).

4. Conclusions

In summary, ethanol oxidation reaction has been investigated in acid and alkaline electrolytes by combining the electrochemical, XPS and *in-situ* IRRAS measurements with DFT calculations. Compared with the Pt foil and 40 wt% Pt/C, the corresponding Pt/TaC thin film and powder catalyst show enhanced EOR activity and stability in both acid and alkaline electrolytes. *In-situ* IRRAS-LSV results suggest a higher CO tolerance and higher CO_2 selectivity on the Pt/TaC surface. DFT calculations reveal that the binding energy of CO is considerably weaker on the Pt/TaC(111) surface, consistent with a higher CO tolerance for Pt/TaC. The binding energies of other possible EOR intermediates are also lower on Pt/TaC(111) than on Pt(111). These factors could explain the enhanced EOR activity observed on the 1.5 wt% Pt/TaC powder catalyst. The combined experimental and theoretical results indicate that Pt-modified TaC should be promising and stable electrocatalysts for EOR in both acid and alkaline electrolytes. These results also provide useful guidelines for the design of carbide-based electrocatalysts for EOR.

Acknowledgements

This work was supported by GEIRI North America, San Jose, California, under State Grid fund SGRI-DL-71-16-015, and by the U.S. Department of Energy, Office of Science, Catalysis Program (DE-FG02-13ER16381). Zhao Jiang acknowledges financial support from the China Scholarship Council (201606285055) and partial support from National Natural Science Foundation of China (No.21706203) and the China Postdoctoral Science Foundation (2016M592794). The DFT calculations were performed using computational resources at the Center for Functional Nanomaterials, a user facility at Brookhaven National Laboratory supported by the U.S. DOE Office of Science under Contract No. DE-AC02-05CH11231.

Appendix A. Supplementary data

Supplementary material related to this article can be found, in the online version, at doi:https://doi.org/10.1016/j.apcatb.2018.04.052.

References

[1] M.A.F. Akhairi, S.K. Kamarudin, Int. J. Hydrogen Energy 41 (7) (2016) 4214–4228.
[2] S. Beyhan, C. Coutanceau, J.-M. Léger, T.W. Napporn, F. Kadırgan, Int. J. Hydrogen Energy 38 (2013) 6830–6841.
[3] Y. Wang, S. Zou, W.-B. Cai, Catalysts 5 (3) (2015) 1507–1534.
[4] N.R. Elezovic, V.R. Radmilovic, N.V. Krstajic, RSC Adv. 6 (8) (2016) 6788–6801.
[5] N.V. Rees, R.G. Compton, Energy Environ. Sci. 4 (4) (2011) 1255.
[6] H. Barthelemy, M. Weber, F. Barbier, Int. J. Hydrogen Energy (2016).
[7] E.G. Mahoney, W. Sheng, M. Cheng, K.X. Lee, Y. Yan, J.G.J. Chen, Power Sources 305 (2016) 89–96.
[8] L.P.R. Moraes, B.R. Matos, C. Radtke, E.I. Santiago, F.C. Fonseca, S.C. Amico, C.F. Malfatti, Int. J. Hydrogen Energy 41 (15) (2016) 6457–6468.
[9] S. Rousseau, C. Coutanceau, C. Lamy, J.-M. Léger, J. Power Sources 158 (1) (2006) 18–24.
[10] J. Xuan, M.K.H. Leung, D.Y.C. Leung, M. Ni, Renew. Sustain. Energy Rev. 13 (6) (2009) 1301–1313.
[11] Z.J. Mellinger, E.C. Weigert, A.L. Stottlemyer, J.G. Chen, Electrochem. Solid-State Lett. 11 (5) (2008) B63.
[12] F. Colmati, G. Tremiliosi-Filho, E.R. Gonzalez, A. Berná, E. Herrero, J.M. Feliu, Faraday Discuss. 140 (2008) 379-97-37.
[13] B.M. Tackett, W. Sheng, J.G. Chen, Joule (2017) 1–11.
[14] E.C. Weigert, A.L. Stottlemyer, M.B. Zellner, J.G. Chen, J. Phys. Chem. C 111 (40) (2007) 14617–14620.
[15] T.G. Kelly, J.G. Chen, Chem. Soc. Rev. 41 (24) (2012) 8021.
[16] A.L. Stottlemyer, P. Liu, J.G. Chen, J. Chem. Phys. 133 (10) (2010) 104702.
[17] T.G. Kelly, A.L. Stottlemyer, X. Yang, J.G. Chen, J. Electrochem. Soc. 161 (8) (2014) E3165–E3170.
[18] D.V. Esposito, J.G. Chen, Energy Environ. Sci. 4 (10) (2011) 3900.
[19] D.V. Esposito, S.T. Hunt, Y.C. Kimmel, J.G. Chen, J. Am. Chem. Soc. 134 (6) (2012) 3025–3033.
[20] Y.C. Kimmel, X. Xu, W. Yu, X. Yang, J.G. Chen, ACS Catal. 4 (5) (2014) 1558–1562.
[21] S.C.S. Lai, S.E.F. Kleijn, F.T.Z. Öztürk, V.C. van Rees Vellinga, J. Koning, P. Rodriguez, M.T.M. Koper, Catal. Today 154 (1) (2010) 92–104.
[22] S.C.S. Lai, M.T.M. Koper, Phys. Chem. Chem. Phys. 11 (44) (2009) 10446–10456.
[23] H.H. Hwu, J.G. Chen, Chem. Rev. 105 (1) (2005) 185–212.
[24] T. Shubina, M.T. Koper, Electrochim. Acta 47 (22–23) (2002) 3621–3628.
[25] S.K. Kim, Y.-J. Zhang, H. Bergstrom, R. Michalsky, A. Peterson, ACS Catal. 6 (3) (2016) 2003–2013.
[26] Y.C. Kimmel, D.V. Esposito, R.W. Birkmire, J.G. Chen, Int. J. Hydrogen Energy 37 (4) (2012) 3019–3024.
[27] G. Kresse, J. Hafner, Phys. Rev. B 47 (1) (1993) 558–561.
[28] G. Kresse, D. Joubert, Phys. Rev. B 59 (3) (1999) 1758–1775.
[29] J.P. Perdew, Y. Wang, Phys. Rev. B 46 (20) (1992) 12947–12954.
[30] L. Ma, D. Chu, R. Chen, Int. J. Hydrogen Energy 37 (15) (2012) 11185–11194.
[31] Busó-Rogero, C., Solla-Gullón, J., Vidal-Iglesias, F. J., Herrero, E., Feliu, J. M.
[32] L. Jiang, A. Hsu, D. Chu, R. Chen, Int. J. Hydrogen Energy 35 (1) (2010) 365–372.
[33] S. John St., A.P. Angelopoulos, Electrochim. Acta 112 (2013) 258–268.
[34] T.G. Kelly, S.T. Hunt, D.V. Esposito, J.G. Chen, Int. J. Hydrogen Energy 38 (14) (2013) 5638–5644.
[35] P.A. Christensen, S.W.M. Jones, A. Hamnett, J. Phys. Chem. C 116 (46) (2012) 24681–24689.
[36] Li, M.; Cullen, D. A.; Sasaki, K.; Marinkovic, N. S.; More, K.; Adzic, R. R. 2012.
[37] P. Gao, S.-C. Chang, Z.J. Zhou, M. Weaver, J. Electroanal. Chem. Interfacial Electrochem. 272 (1) (1989) 161–178.
[38] E.K. Plyler, J. Res. Natl. Bur. StanJards 48 (4) (1952).
[39] K. Arihara, F. Kitamura, T. Ohsaka, K. Tokuda, J. Electroanal. Chem. 510 (1) (2001) 128–135.
[40] P.A. Christensen, A. Hamnett, D. Linares-Moya, Phys. Chem. Chem. Phys. Phys. Chem. Chem. Phys 13 (13) (2011) 11739–11747.
[41] T. Iwasita, E. Pastor, Ekctrochimica Acta 39 (4) (1994) 531–537.
[42] G.A. Camara, R.B. de Lima, T. Iwasita, J. Electroanal. Chem. 585 (1) (2005) 128–131.
[43] Y. Holade, N. Sahin, K. Servat, T. Napporn, K. Kokoh, Catalysts 5 (1) (2015) 310–348.
[44] G.A. Camara, T. Iwasita, J. Electroanal. Chem. 578 (2) (2005) 315–321.
[45] M. Li, D.A. Cullen, K. Sasaki, N.S. Marinkovic, K. More, R.R. Adzic, J. Am. Chem. Soc. 135 (1) (2013) 132–141.
[46] Z.-Y. Zhou, Q. Wang, J.-L. Lin, N. Tian, S.-G. Sun, Electrochim. Acta 55 (27) (2010) 7995–7999.
[47] P.A. Christensen, D. Linares-Moya, J. Phys. Chem. C 114 (2) (2010) 1094–1101.
[48] E.A. Monyoncho, S.N. Steinmann, C. Michel, E.A. Baranova, T.K. Woo, P. Sautet, ACS Catal. 6 (8) (2016) 4894–4906.
[49] H.F. Wang, Z.P. Liu, J. Am. Chem. Soc. 130 (33) (2008) 10996–11004.
[50] G. Cui, P.K. Shen, H. Meng, J. Zhao, G. Wu, J. Power Sources 196 (15) (2011) 6125–6130.